RSC Advances

ROYAL SOCIETY OF CHEMISTRY

www.rsc.org/advances

Journal Name

RSCPublishing

ARTICLE

Anomalous Effects of Water Flow through Charged Nanochannel Membranes

Cite this: DOI: 10.1039/x0xx00000x

Received 00th January 2012,
Accepted 00th January 2012

DOI: 10.1039/x0xx00000x

www.rsc.org/

Meng Yang, Xiaohai Yang*, Qing Wang, Kemin Wang*, Xin Fan, Wei Liu, Xizhen Liu, Jianbo Liu, Jin Huang

A nanoscale understanding of water transport is crucial to gaining fundamental insight into the biological systems and improving the design of engineering systems. Herein, anomalous effects of water flow were observed in our experiment by measuring the net flux of water through charged nanochannel membranes that separated pure water from electrolyte solution. The direction and flux of water transport can be controlled as a function of nanochannel surface charge, electrolyte concentration and electrolyte type. For some electrolyte types in the proper concentration range, the net flux of water transport was from electrolyte solution to pure water, which is an anomalous osmosis phenomenon and violates van't Hoff's law. In order to explain the anomalous effect, a concise model was put forward. According to the model, the direction and flux of water transport were the results of combining concentration diffusion with induced electroosmosis under certain electrolyte gradient. In addition, neutral molecule transport, and ionic species separation through charged nanochannel membranes can also be modulated by adjusting the electrolyte gradient. These results suggest that polyelectrolyte modified nanochannel membranes have good potential for application as a kind of nanovalve under electrolyte gradient.

1 Introduction

Studies of mass transport in nanoscale will contribute to our understanding of the underlying transport mechanisms and developing nanofluidic devices.[1-5] Mass transport in nanoscale differs greatly from those of bulk-scale, since various surface or interfacial forces including steric interactions, van der Waals forces and electrostatic forces become important due to the large surface-to-volume ratios.[6-9] For example, in nanochannels, channel dimensions are narrowed to electrical double layer (EDL) thickness.[10] Usually, the overlapping of EDL is very significant, leading to various unique properties including ion selectivity,[11-13] local ion depletion/enrichment,[14-16] active gated control of ions/molecules,[17-23] ionic current rectification[24-28] and energy conversion from streaming current.[29-31] Thus, novel transport properties on the nanoscale are expected to emerge from the combination of the strong confinement and the unique surface properties.

In recent years, with the advances in processing technology of artificial nanochannel preparation, as well as some new means of detection in experiments, there have been some interesting reports on mass transport phenomena in nanoscale. Holt et al. reported fast mass transport through sub-2-nanometer carbon nanotubes.[32] They found that water permeabilities in carbon nanotubes with diameters of less than 2 nm are several orders of magnitude higher than those of commercial polycarbonate membranes, despite having pore sizes an order of magnitude smaller. Chmiola et al found that decreasing the pore size to less than 1 nm led to an anomalous increase in carbon capacitance.[33] Lee et al observed water flow enhancement in hydrophilic nanochannels.[34] Duan et al. reported that the mobility of ions restricted in 2 nm hydrophilic nanochannels was faster than that in bulk phase, and proton mobility increased four times over the bulk value at low concentration.[35] Chinen et al. observed that proton mobility was enhanced in the extended-nanospace channels from 570 nm to 180 nm by using a pH-sensitive fluorescent probe to monitor the proton diffusion in the extended-nanospace channels.[36] This phenomenon cannot be explained by the change in the viscosity of water because water confined in the extended nanospaces has a higher viscosity compared with bulk water.[37] Chen et al. reported anomalous diffusion of electrically neutral molecules in charged nanochannels. For the first time, they found that the diffusion flux of phenol, a neutral molecular, varied with the ionic strength in 20 nm alumina nanochannels.[38] These anomalous transport phenomena mostly stem from interactions between the transported mass and the nanochannel walls.

Numerical simulation is also contributed to our understanding of mass transport in the nanoscale. Several recent numerical researches have showed that anomalous osmosis, i.e. water flow through charged nanochannels from higher electrolyte concentration to lower electrolyte concentration, can occur.[39-41] This inference is interesting

and can offer some basic explanations of the translocation of liquids across biological membranes, since some phenomena of liquid transport through biological membranes cannot be explained on the basis of the concept of normal van't Hoff osmosis.[42,43] However, up to now, experimental investigations based on charged nanochannels are still scarce. Thus, it is important to investigate mass transport through charged nanochannels by experiment for clarifying the anomalous water transport mechanisms in nanoscale.

Here, we provided an experimental study of anomalous osmosis phenomenon for artificial charged nanochannel membranes. The charged nanochannel membranes were fabricated by depositing layer-by-layer assembled polyelectrolyte multilayers comprising poly (allylamine hydrochloride) (PAH) and poly (sodium 4-styrenesulfonate) (PSS) in 100 nm track-etched polycarbonate membranes (TEPC) (see Figure S1). A concise model was established to describe the conditions of anomalous osmosis. It pointed out that the direction and net flux of water transport were decided by concentration diffusion and induced electroosmosis. When the direction of concentration diffusion and induced electroosmosis was opposite, anomalous osmosis could occur under certain electrolyte gradient. The direction and net flux of water transport were investigated under different conditions, including electrolyte concentrations, electrolyte types and the charge of nanochannel membranes. The results showed that the inferences of model were consistent with experimental data. In addition, according to the model, neutral molecular transport and ionic species separation can be modulated by adjusting the electrolyte gradient. To demonstrate this, the electrically neutral molecule (phenol) and ionic species (methylviologen (MV^{2+}) dichloride and 1, 5-naphthalene disulfonate (NDS^{2-}) disodium salt) were selected as models.

2 Model of Transport

To explore the transport of water through the charged nanochannel membranes under electrolyte gradient, a transport model was put forward. As shown in Figure 1, water transport is composed of concentration diffusion and induced electroosmosis, the net flux of water transport is the net result of the two parts. According to difference of nanochannel surface charge and electrolyte type, the transport model can be divided into four kinds of situations, which are showed in Figure 1a-d. To illustrate our model, we employed Figure 1a as an example, i.e. a negatively charged nanochannel membrane connected two half-cells which contained electrolyte solution and pure water, respectively.

Obviously, according to the van't Hoff's law, there would be a water transportation from the pure water to electrolyte solution, which is induced by concentration diffusion. Such water transport is represented by the green arrow pointing left in Figure 1a, marked as F_{cd}.

In addition, water transport is also caused by induced electroosmosis. However, the generation of induced electroosmosis is more complex than F_{cd}. As shown in Figure 1a, according to two-region model mentioned by Chen et al, electrostatic interaction region and free transport region exist in the nanochannel.[38, 44]

For a negatively charged nanochannel, the channel surface can attract cations (M^+), forming electric double layer (EDL), and repel anions (A^-) due to the electrostatic interactions. Diffusion of anions (A^-) through the nanochannels mainly occurs in the free transport region under the electrolyte gradient. Since the diffusion coefficient of the anion (A^-) is larger than that of the cation (M^+), the anions can pass channel more quickly. This causes anions (A^-) to accumulate faster in the pure water half-cell. As a result, a membrane diffusional potential is formed between the two half-cells. The membrane diffusional potential, which acting on the cations accumulated in the EDL, induces water transport referred to as induced electroosmosis. Such water transport is represented by the orange arrow pointing right in Figure 1a, marked as F_{ie}. The direction of induced electroosmosis is towards pure water half-cell.

As shown in Figure 1a, the direction of F_{cd} and F_{ie} is opposite. If F_{ie} is larger than F_{cd}, the net result is that the water transport from electrolyte solution to pure water, and anomalous osmosis phenomena may be observed. Therefore, if we change the electrolyte type and nanochannel surface charge, anomalous osmosis phenomena can be controlled:

As shown in Figure 1b, for the negatively charged nanochannel, if the diffusion coefficient of the cation (M^+) is larger than that of the anion (A^-), the direction of F_{cd} is the same with the direction of F_{id}. Water always transport from pure water toward electrolyte solution. Anomalous osmosis phenomena cannot be observed.

As shown in Figure 1c, for the positively charged nanochannel, if the diffusion coefficient of the anion (A^-) is larger than that of the cation (M^+), the direction of F_{cd} is the same with the direction of F_{id}. Water always transport from pure water toward electrolyte solution. Anomalous osmosis phenomena cannot be observed.

As shown in Figure 1d, for the positively charged nanochannel, if the diffusion coefficient of the cation (M^+) is larger than that of the anion (A^-), the direction of F_{cd} is opposite to the direction of F_{id}. Anomalous osmosis phenomenon may be observed.

In order to provide evidence to prove the four inferences from the model, the net flux and direction of water transport were investigated by experimental approach under different conditions, including electrolyte concentrations, electrolyte types and nanochannel surface charge. The setup for water transport experiment was shown in Figure 2 and Figure S4.

3 Materials and Methods

3.1 Materials

Poly (sodium 4-styrenesulfonate) (PSS) (M_w=70 000) and poly (allylamine hydrochloride) (PAH) (M_w=56 000) were purchased from Aldrich and used as received. Methylviologen (MV^{2+}) and 1, 5-naphthalene disulfonate (NDS^{2-}) were purchased from TCI and used as received. Phenol, lithium chloride, sodium chloride, potassium chloride, calcium chloride, magnesium chloride, barium chloride, hydrochloric acid, nitrate, sulfuric acid, and phosphate were purchased from Xilong reagent company (Guangdong China). Track-etched polycarbonate membranes (TEPC, 6 μm thickness, 25 mm diameter) whose pore diameters are 100 nm were purchased from Osmonics. All solutions were prepared with ultrapure Milli-Q water (Resistance > 18.2 MΩ.cm^{-1}).

3.2 Modification of Track-Etched Polycarbonate Membranes with Polyelectrolyte Multilayers

Polyelectrolyte solutions at a concentration of 1 mg/mL were prepared in 100 mM acetate buffer (pH~4.7) under conditions of full protonation of the PAH. All solutions were freshly prepared before use.[45]

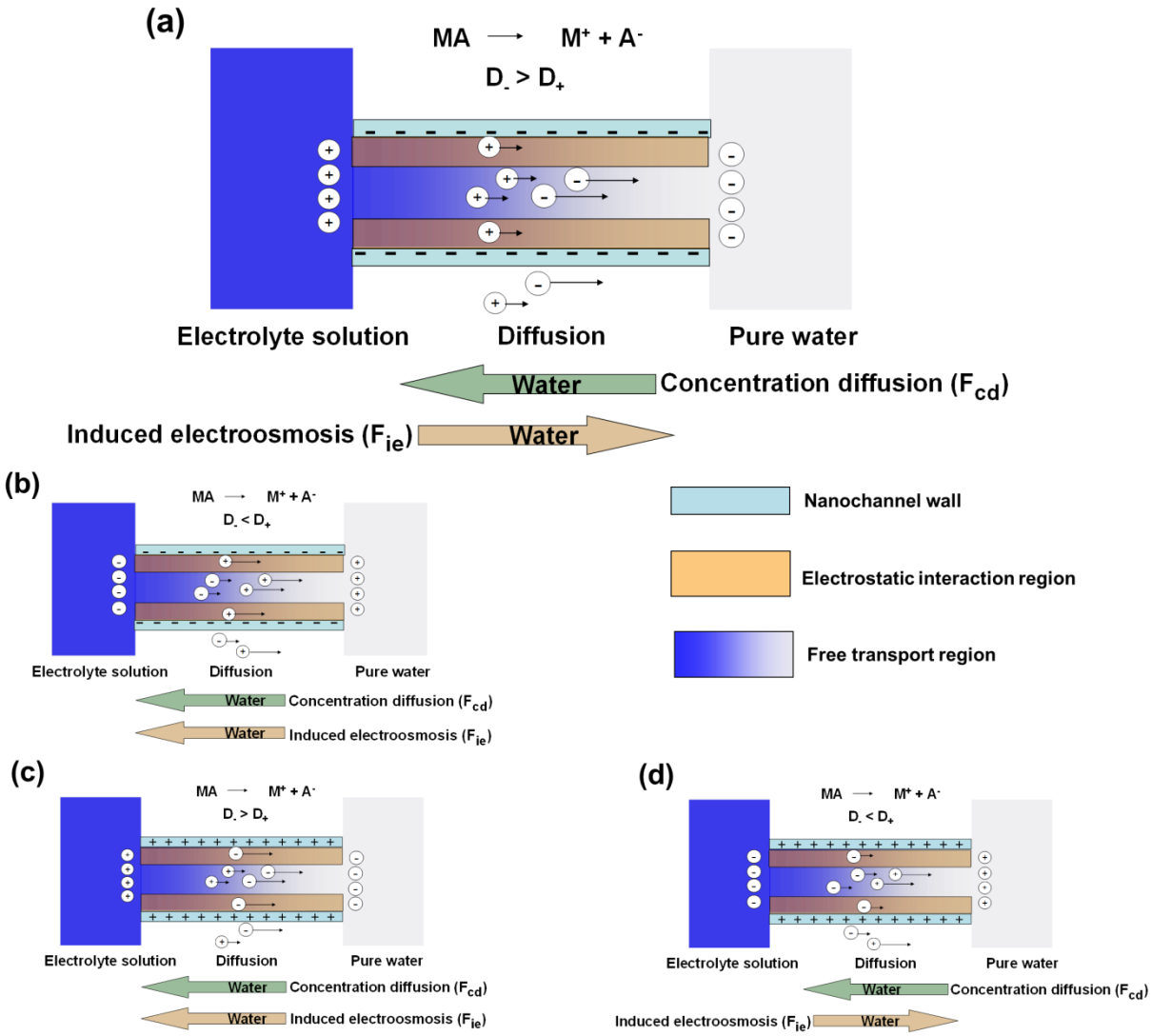

Figure 1. Schematic of water transport across charged nanochannel membranes. MA, M^+, A^-, D_+ and D_- represent respectively electrolyte, cation, anion, cation diffusion coefficient and anion diffusion coefficient; Green arrow pointing represents the direction of water transport induced by electrolyte concentration diffusion, Orange arrow pointing represents the direction of water transport due to induced electroosmosis.

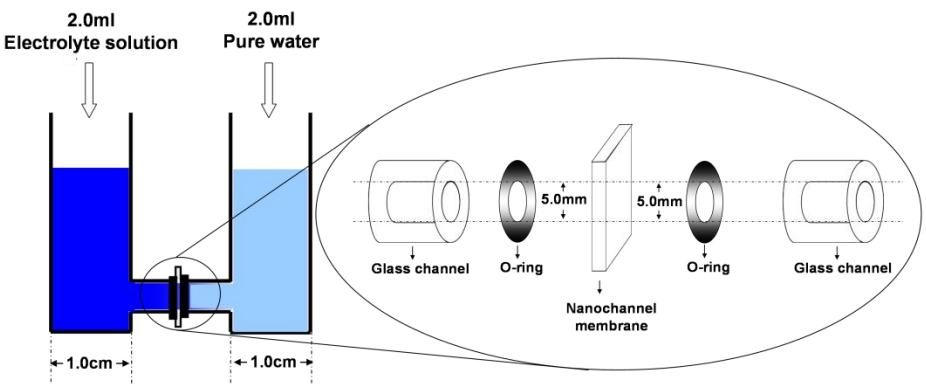

Figure 2. Schematic representation of setup for water transport experiments. The liquid volume of each half-cell was 2.0 ml at the beginning of the experiments.

A track-etched polycarbonate membrane was immersed into methanol for 5 min and then immersed for 45 min in a solution that was 25 mM in $SnCl_2$ and 70 mM in trifluoroacetic acid. The membrane was then washed in methanol two consecutive times for 2.5 min each.[46] This yields the Sn-sensitized form of the membrane that was then used for the preparation of charged nanochannel membrane. This membrane was then placed in a filter holder and polyelectrolyte multilayers were deposited by filtering the polyanion (PSS) solution and the polycation (PAH) solution alternately in vacuum. Each filtration process was repeated three times, and copious amounts of water were used to remove any unabsorbed polymer before next filtering a polyelectrolyte solution. In this way, both negatively and positively charged nanochannels can be obtained.[47]

3.3 Electron Microscopy characterization of Multilayer Nanochannel Membranes

To measure the multilayer growth in pores of track-etched polycarbonate membranes, scanning electron microscopy (SEM) and cross-section transmission electron microscopy (TEM) were performed. SEM images were obtained using a JSM-6700 operated at 5.0 kV. For TEM, the membranes were dissolved in dichloromethane with subsequent sonication for less than 30 s. The extracted nanotubes were then collected on TEM carbon grids and imaged with a JEOL-JEM operated at 100 keV.[45]

3.4 Measure of Water Flux

To study the transport of water, the membrane was mounted between two half-cells. The experimental setup is schematically depicted (Figure S4). Typically, 2.0 mL electrolyte solution was placed on one half-cell, and 2.0 mL pure water was placed on the other half-cell, keeping the same liquid level in two half-cells at the beginning of the experiments.

After 12 h, differences in liquid levels were observed due to water transport. The liquid levels in two half-cells were measured using DSA100 Contact Angle Measuring System (KRÜSS) (positioning accuracy=0.1 mm) (Figure S4b).

Then the difference of liquid levels can be converted to net flux of water transport using the equation:

$$J_w = \frac{A_c\left(\frac{\Delta h}{2}\right)\rho}{M_w t A_m}\times 10^6 \qquad (1)$$

where J_w is the water flux (μmol min^{-1} cm^{-2}), A_c is the cross sectional area of half-cell (0.25π cm^2), Δh is the difference of liquid level (cm), ρ is the density of water (1.0 g/mL), M_w is the molar mass of water (18 g/mol), t is the penetration time (min), A_m is the area of nanochannel membrane (π/16 cm^2).

3.5 Measure of Phenol-Diffusion Flux

The phenol flux was determined by monitoring the concentration change of phenol at the permeation half-cell. This was accomplished by UV detection of the permeation solution with a UV/Vis spectrophotometer (UV-1601, SHIMADZU) at 270 nm. The absorbance data were converted to concentration of phenol.

The phenol flux was calculated from the experimental date using the equation:

$$J_{PhOH} = \frac{VC_{PhOH}}{tA_m}\times 10^6 \qquad (2)$$

where J_{PhOH} is the phenol flux (nmol min^{-1} cm^{-2}), V is the volume of solution at the permeation half-cell (mL), C_{PhOH} is the phenol concentration (mol L^{-1}) at the permeation half-cell, t is the penetration time (min), A_m is the area of nanochannel membrane (π/16 cm^2).

3.6 Separation of MV^{2+} and NDS^{2-}

The flux of MV^{2+} and NDS^{2-} was determined by monitoring the concentration change of MV^{2+} and NDS^{2-} at the permeation half-cell. This was accomplished by UV detection of the permeation solution with a UV/Vis spectrophotometer (UV-1601, SHIMADZU) at 225 nm and 257 nm. The absorbance data were converted to concentration of MV^{2+} and NDS^{2-}.

The flux of MV^{2+} and NDS^{2-} were calculated using the equations:

$$J_{MV^{2+}} = \frac{VC_{MV^{2+}}}{tA_m}\times 10^6 \qquad (3)$$

and

$$J_{NDS^{2-}} = \frac{VC_{NDS^{2-}}}{tA_m}\times 10^6 \qquad (4)$$

where $J_{MV}{}^{2+}$ and $J_{NDS}{}^{2-}$ are the flux of MV^{2+} and NDS^{2-} (nmol min^{-1} cm^{-2}) respectively, V is the volume of solution at the permeation half-cell (mL), $C_{MV}{}^{2+}$ and $C_{NDS}{}^{2-}$ are the concentration of the MV^{2+} and NDS^{2-} (mol L^{-1}) in permeate solution after permeating 3 h respectively, t is the penetration time (min), A_m is the area of nanochannel membrane (π/16 cm^2).

4 Results and Discussion

4.1 Water Transport through 3.5(PSS/PAH) Coated 100nm Nanochannel Membranes under Different LiCl Concentration

According to the van't Hoff's law, electrolyte concentration can affect on F_{cd}. The size of electrostatic interaction region and free transport region in transport model is also related to electrolyte concentration. This is because the size of the electric double layer is characterized by the Debye screening length. The ion concentration η and the Debye screening length l_D follow the relation $l_D \propto 1/\sqrt{\eta}$.[35] Therefore, electrolyte concentration is an important factor to water transport.

To study the effect of electrolyte concentration on water transport, 3.5(PSS/PAH) coated 100 nm nanochannel membrane, a negatively charged nanochannel membrane, was used, and LiCl was selected because diffusion coefficient of Cl^- (2.032×10^{-5} cm^2s^{-1}) is bigger than that of Li^+ (1.029×10^{-5} cm^2s^{-1}). Solutions of LiCl in the concentration range from 0 to 1000 mM were investigated. LiCl solution and pure water were separated by 3.5(PSS/PAH) coated 100 nm nanochannel membrane. The net flux and direction of water transport were determined by measuring the liquid levels in two half-cells after 12 h. The difference of liquid levels was converted to the net flux of water transport using the relation in Equation 1. Figure 3 showed the net flux and direction of water transport through the nanochannel membranes as a function of bulk LiCl concentrations.

When the bulk LiCl concentration was relatively low, the water transported from the pure water side towards the LiCl solution side. The net flux of water increased with the increase of LiCl concentration. This was because electrostatic interaction region was large and free transport region was small, even inexistent at a relatively low concentration due to electric

double layer overlap. It was difficult for Cl^- ions to pass by the channels. Water transport was mainly dominated by F_{cd} from pure water to LiCl solution.

However, as the bulk LiCl concentration further increased, the net water flux towards LiCl solution decreased. Once the bulk LiCl concentration exceeded 10 mM, the direction of the net flux of water was changed, and anomalous osmosis was observed. Subsequently, the net water flux towards pure water increased with the increase of LiCl concentration. When the LiCl concentration increased to 50 mM, the net flux of water attained a maximum, and anomalous osmosis was most obvious. This can be explained as follows: as the bulk LiCl concentration further increased, the EDL gradually became thin, and free transport region gradually increased. Cl^- ions can quickly pass channel by free transport region, and form membrane diffusional potential. The membrane diffusional potential acting on Li^+ accumulated in the EDL produced F_{ie} towards pure water. Although F_{cd} and F_{ie} increased with the increase of LiCl concentration, the increase of F_{ie} was faster than F_{cd} in this concentration range. As a result of competition with F_{cd} and F_{ie}, the direction of net flux of water changed from LiCl solution to pure water.

Above this optimal value, the net water flux toward pure water decreased as the LiCl concentration increased. Finally the direction of the net flux of water was changed again. This was because water transport was mainly determined by F_{cd} with the increase of LiCl concentration. These results clearly showed that the net flux and direction of water transport can be modulated as a function of LiCl concentration.

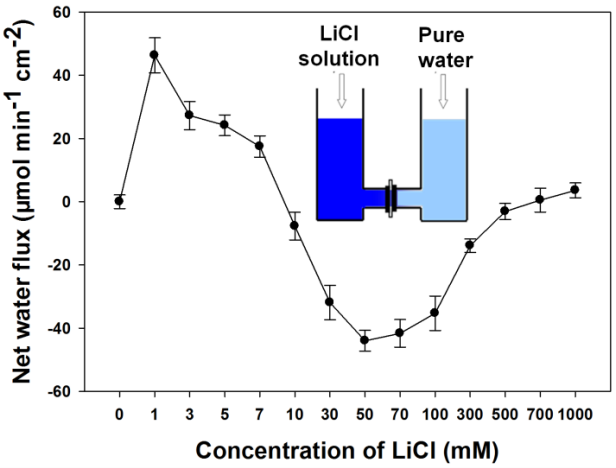

Figure 3. The net flux of water transport as a function of LiCl concentration. A negative value indicates that the direction of the net flux of water is toward pure water. The data corresponding to water transport through the 3.5(PSS/PAH) coated 100 nm nanochannel membranes after standing 12 h at 20 °C.

4.2 Effect of Nanochannel Diameter on Water Transport under 50 mM LiCl Concentration

The above results indicated that the nanochannel diameter has important effect on water transport, since the size of free transport region was different for the charged nanochannel of different diameter under the same electrolyte concentration. To investigate the effect of nanochannel diameter on water transport, different numbers of (PSS/PAH) multilayers were deposited onto 100 nm pore TEPC membranes.

SEM images of the pores at various stages of multilayer deposition showed that the diameter of pores decreased with the increasing number of multilayer, and no clogging was observed up to 4.5(PSS/PAH) (see Figure S2). In order to ascertain that n(PSS/PAH) multilayers were modified through the full length of the nanochannels, 3.5(PSS/PAH) coated 100 nm nanochannel membrane was treated with dichloromethane to liberate the (PSS/PAH) multilayers. The TEM images of the liberated (PSS/PAH) multilayer nanostructures clearly showed that the modified multilayers were assembled in the interior of the nanochannels (see Figure S3).

Experiments of water transport through n(PSS/PAH) multilayers (n=0 to 4.5) were conducted under 50 mM LiCl, as shown in Figure 4. When n=3.5, the net flux of water toward the direction of pure water was the biggest, and the anomalous osmosis was most obvious. This was because the proportion of electrostatic interaction region and free transport region was different due to the difference of nanochannel diameter. In the following experiments, the 3.5(PSS/PAH) coated 100 nm nanochannel membranes was selected as the negatively charged nanochannel to study the effect of electrolyte type and non-electrolyte substances on water transport.

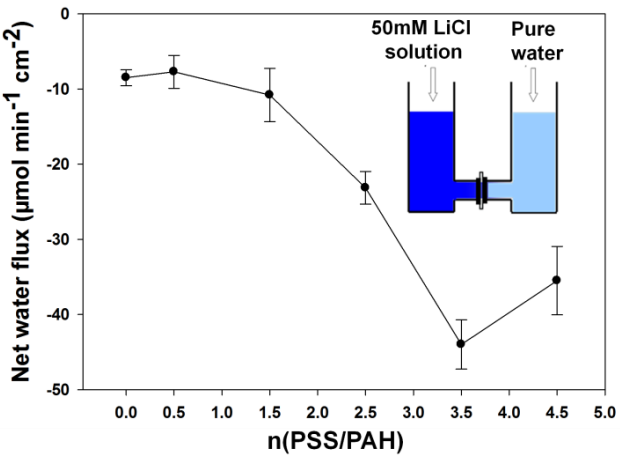

Figure 4. The net flux of water transport as a function of n(PSS/PAH). A negative value indicates that the direction of the net flux of water is toward pure water. The data corresponding to water transport through the n(PSS/PAH) coated 100 nm nanochannel membranes after standing 12 h at 20 °C.

4.3 Water Transport through 3.5(PSS/PAH) Coated 100 nm Nanochannel Membranes under Different Electrolyte Types

According to our model shown in Figure 1a, the diffusion coefficient difference of anion (A^-) and cation (M^+) will also affect on water transport because the membrane diffusional potential, as a driving force of F_{ie}, is closely related to the diffusion coefficient difference of anion (A^-) and cation (M^+).

To prove this, electrolyte solutions of 50 mM LiCl, NaCl, KCl, $MgCl_2$, $CaCl_2$, $SrCl_2$ and $BaCl_2$ were first used for the investigation of water transport. As shown in Figure 5, the water transport towards pure water gradually decreased from LiCl to NaCl to KCl, and from $MgCl_2$ to $CaCl_2$ to $SrCl_2$ to $BaCl_2$. Obviously, the tendency was the same as that of diffusion coefficient difference in Table S1. The results were consistent with inference of transport model shown in Figure 1a.

Then, electrolyte solutions of 50 mM HCl, HNO_3, H_2SO_4, and H_3PO_4 were used for the investigation of water transport. As shown in Figure 6, for the 3.5(PSS/PAH) coated 100 nm nanochannel membranes, since the diffusion coefficient of the cation (H^+) was larger than that of the anion (acid radical), the direction of F_{cd} was the same with F_{id}. Water always transported from pure water toward acid solution. Anomalous

osmosis phenomena could not be observed. The results were consistent with inference of the model shown in Figure 1b.

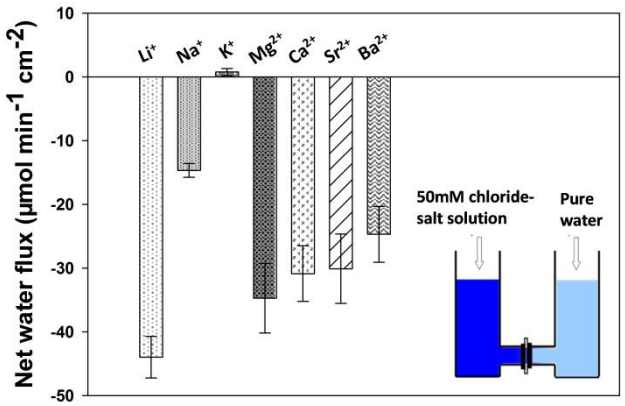

Figure 5. The net flux of water transport as a function of different electrolyte types. A negative value indicates that the direction of the net flux of water is toward pure water. The data corresponding to water transport through the 3.5(PSS/PAH) coated 100 nm nanochannel membranes after standing 12 h at 20 °C.

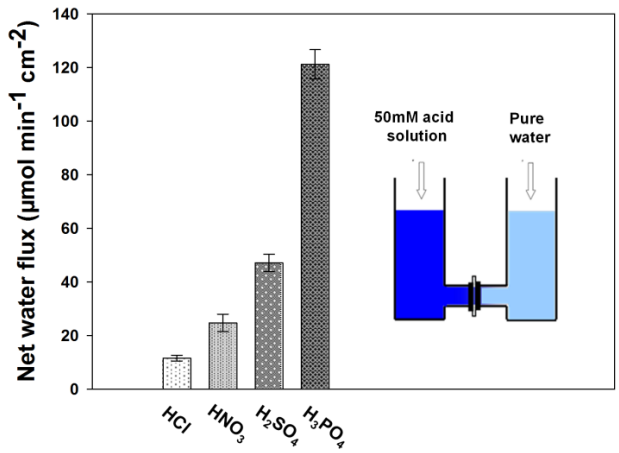

Figure 6. The net flux of water transport as a function of different electrolyte types. A positive value indicates that the direction of the net flux of water is toward acid solution. The data corresponding to water transport through the 3.5(PSS/PAH) coated 100 nm nanochannel membranes after standing 12 h at 20 °C.

4.4 Water Transport through 4.0(PSS/PAH) Coated 100 nm Nanochannel Membranes under Different electrolyte types

According to our model, if positively charged nanochannel membrane was used for water transport under different electrolyte, inverse situation should be observed.

To prove this, 4.0(PSS/PAH) coated 100 nm nanochannel membranes were selected due to the positively charged surface, and electrolyte solutions of 50 mM LiCl, NaCl, KCl, $MgCl_2$, $CaCl_2$, $SrCl_2$ and $BaCl_2$ were used for the investigation of water transport. As shown in Figure 7, water transported from pure water to chloride-salt solution. The results were opposite to that of 3.5(PSS/PAH) coated 100 nm nanochannel membrane, and was consistent with the inference of model shown in Figure 1c.

The same situation also happened when 50 mM HCl, HNO_3, H_2SO_4, and H_3PO_4 were used for the investigation of water transport. As shown in Figure 8, water transported from acid solution to pure water. The results were also opposite to that of 3.5(PSS/PAH) coated 100 nm nanochannel membrane, and was consistent with the inference of model shown in Figure 1d.

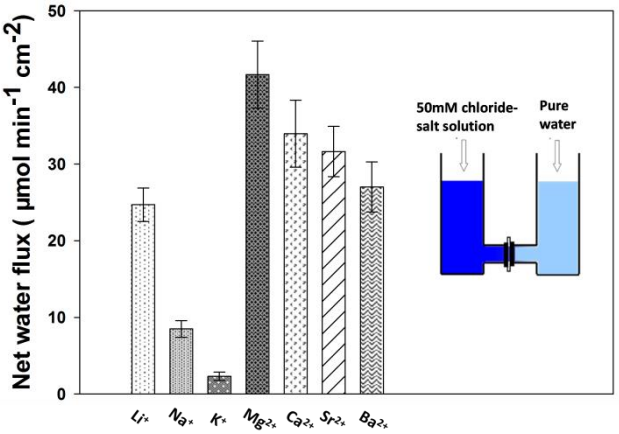

Figure 7. The net flux of water transport as a function of different electrolyte types. A positive value indicates that the direction of the net flux of water is toward chloride-salt solution. The data corresponding to water transport through the 4.0(PSS/PAH) coated 100 nm nanochannel membranes after standing 12 h at 20 °C.

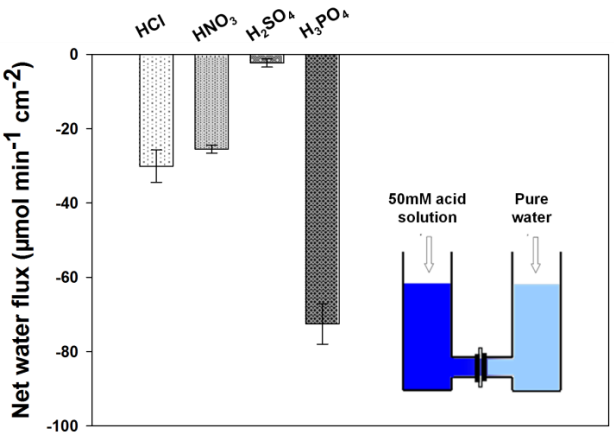

Figure 8. The net flux of water transport as a function of different electrolyte types. A negative value indicates that the direction of the net flux of water is toward pure water. The data corresponding to water transport through the 4.0(PSS/PAH) coated 100 nm nanochannel membranes after standing 12 h at 20 °C.

4.5 Water Transport through 3.5(PSS/PAH) and 4.0(PSS/PAH) Coated 100 nm Nanochannel Membranes under Non-Electrolyte Solution

According to our model, non-electrolyte substances, which could not be ionized in aqueous solution and form membrane diffusional potential, should not produce F_{ie} under concentration gradient. Regardless of the nanochannel surface

charge, water transport was determined by F_{cd} from pure water to non-electrolyte solution.

To prove this, experiments of water transport through the 3.5(PSS/PAH) and 4.0(PSS/PAH) coated 100 nm nanochannel membranes were performed using 100 mM solution of glucose and γ-cyclodextrin. The net flux and direction of water transport were given in Figure 9. Water transported from pure water toward non-electrolyte solution. Anomalous osmosis phenomena could not be observed.

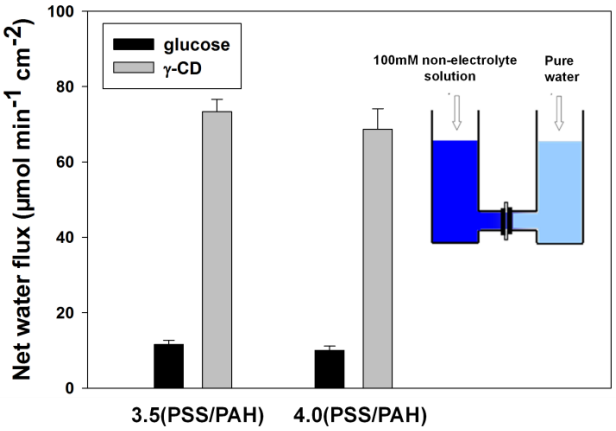

Figure 9. The net flux of water transport in the present of non-electrolytes. A positive value indicates that the direction of the net flux of water is toward non-electrolyte solution The data corresponding to water transport through 3.5(PSS/PAH) and 4.0(PSS/PAH) coated 100 nm nanochannel membranes after standing 12 h at 20 °C.

4.6 Neutral Molecular Transport through 3.5(PSS/PAH) Coated 100 nm Nanochannel Membranes under Salt Gradient

Modulating and controlling the mass transport across nanochannels are of great importance for designing novel molecular devices, machines and sensors. Here F_{ie} as a form of liquids transport, caused by the interplay of membrane diffusional potential and EDL, should be useful to modulate neutral molecular transports.

To demonstrate that it is possible to modulate the transport of neutral molecule by F_{ie}, phenol, a neutral molecule commonly used as an indicator in studies of mass-transport behavior in nanochannels, [38] was selected as the model molecule. The flux of phenol was determined by the relation in Equation 2. Figure 10 showed the distinct diffusion behavior of phenol through 3.5(PSS/PAH) coated 100 nm nanochannel membranes under different conditions.

As shown in Figure 10, in the case of no salt gradient, the diffusion flux of phenol corresponding to condition (b) was larger than that of the condition (a). The difference of flux can be explained by the size change of free transport region and electrostatic interaction region. As 50 mM LiCl was added, the free transport region expanded while electrostatic interaction region shrinked. The expansion of free transport region was to facilitate the diffusion of phenol, since the diffusion of phenol was slow in electrostatic interaction region due to the interaction between the inductive dipole of phenol and the negatively charged surface.[38]

When the salt gradient was established under condition (c), the diffusion flux of phenol further increased compared with the condition (b). This can be explained by our model as shown in Figure 1a. Under condition (c), the direction of F_{ie} was from feed half-cell to permeation half-cell, and then the direction of net water flux was toward permeation half-cell. Therefore, the direction of phenol diffusion was consistent with the direction of F_{ie}, which promoted the transport of phenol through the nanochannel membranes.

These studies clearly demonstrated that the F_{ie} could be utilized to modulate the transport rate of neutral molecule through the charged nanochannel membranes.

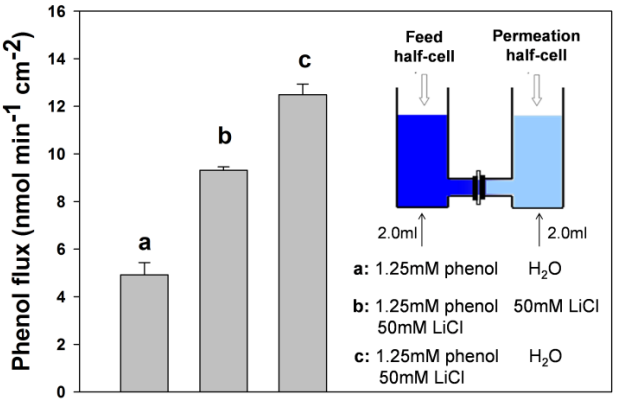

Figure 10. The net flux of phenol transport through 3.5 (PSS/PAH) coated 100 nm nanochannel membranes after stirring 3 h at 20 °C. A positive value indicates that the direction of the net flux of phenol is toward permeation half-cell.

4.7 Separation of Ionic Species Using 3.5(PSS/PAH) Coated 100 nm Nanochannel Membranes under Salt Gradient

The permeation of ionic species through charge nanochannel membranes is common in many biophysical systems and biotechnological applications. According to our model, the membrane diffusional potential, caused by the asymmetric diffusion between cations and anions, had action on ionic species leading to induced electrophoresis. The collaboration between induced electroosmosis and induced electrophoresis can be further employed to improve the separation selectivity of different charged molecules.

In order to investigate the effect of the induced electroosmosis and induced electrophoresis on ionic species separation, MV^{2+} and NDS^{2-} were selected as model cation and anion, since they were both divalent ion and had similar molecular volumes.[48] This ensured that the separation of MV^{2+} and NDS^{2-} was based on charge difference rather than volume difference.

Figure 11 showed the separation selectivity of the mixed solution of MV^{2+} and NDS^{2-} through 3.5(PSS/PAH) coated 100 nm nanochannel membranes under different conditions. The separation selectivity *S* was defined as

$$S = \frac{J_{MV^{2+}}}{J_{NDS^{2-}}} \qquad (5)$$

where $J_{MV}{}^{2+}$ and $J_{NDS}{}^{2-}$ represent the fluxes of MV^{2+} and NDS^{2-} respectively (see Equation 3 and 4).

As shown in Figure 11, in the case of no salt gradient, the diffusion flux of MV^{2+} and NDS^{2-} corresponding to condition (b) was larger than that of the condition (a), but the change of *S* of MV^{2+} was not obvious. This phenomenon could also be explained by the size change of free transport region and electrostatic interaction. Due to adding 50 mM LiCl, the free transport region expanded, and then the flux of MV^{2+} and NDS^{2-} increased from condition (a) to condition (b).

When salt gradient was established under condition (c), the separation selectivity *S* further increased. The improvement of separation selectivity could also be explained by our model as shown in Figure 1a. Under salt gradient, membrane diffusional potential was formed due to different diffusion of Li^+ and Cl^-. For MV^{2+}, the direction of induced electroosmosis and induced electrophoresis was the same as that of the diffusion. For NDS^{2-}, only the direction of induced electroosmosis was the same as that of the diffusion. Therefore, the flux of MV^{2+} was dramatically higher than that of NDS^{2-}.

The results clearly demonstrated that the membrane diffusional potential could be utilized to improve the separation selectivity of ionic species in charged nanochannel membranes.

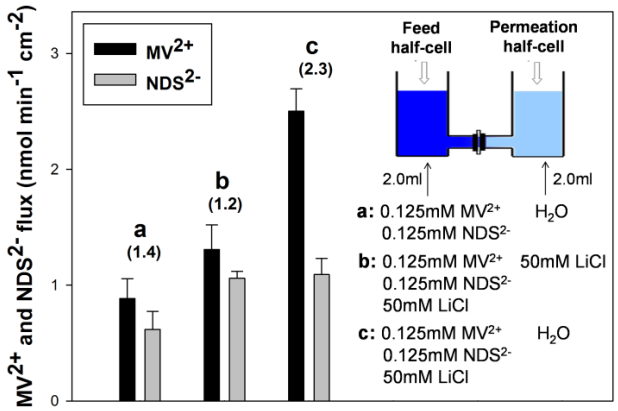

Figure 11. The net flux of MV^{2+} and NDS^{2-} through 3.5(PSS/PAH) coated 100 nm nanochannel membranes after stirring 3 h at 20 °C. A positive value indicates that the direction of the net flux of MV^{2+} and NDS^{2-} is toward permeation half-cell. The date above the histogram is correspond to separation selectivity *S* of MV^{2+}.

5 Conclusions

In summary, we have presented anomalous effects of water flow through charged nanochannel membranes. A concise model was established to describe the conditions of anomalous effects. According to the model, water transport was composed of concentration diffusion and induced electroosmosis under electrolyte gradient. The direction and net flux of water transport were sensitive to nanochannel surface charge, electrolyte concentration and electrolyte type, which were confirmed by experiments. In addition, we have also demonstrated that the transport of electrically neutral molecules and the separation selectivity of ionic species through charged nanochannel membranes can be modulated by adjusting electrolyte gradient. These results may deepen our understanding of mass transport in the nanoscale and may also be helpful in the development of nanofluidic devices. From a perspective of potential application, it may be possible for polyelectrolyte modified nanochannel membranes to develop into a kind of nanovalve under electrolyte gradient.

Acknowledgments

This work was supported by the National Natural Science Foundation of China (21190040, 21175035, 21375034), National Basic Research Program (2011CB911002), International Science & Technology Cooperation Program of china (2010DFB30300).

Notes and references

State Key Laboratory of Chemo/Biosensing and Chemometrics, College of Chemistry and Chemical Engineering, Key Laboratory for Bio-Nanotechnology and Molecular Engineering of Hunan Province, Hunan University, Changsha 410082, P. R. China. Fax: 86-731-88821566; Tel: 86-731-88821566; E-mail: kmwang@hnu.edu.cn, yangxiaohai@hun.edu.cn

† Electronic Supplementary Information (ESI) available: Number of deposited n(PSS/PAH) multilayer, SEM images of n(PSS/PAH) multilayer, TEM images of 3.5(PSS/PAH) nanotubes, Experimental system used to measure the liquid levels, Ionic conductivity and diffusion coefficient. See DOI: 10.1039/b000000x/

1 F. Fornasiero, H. G. Park, J. K. Holt, M. Stadermann, C. P. Grigoropoulos, A. Noy and O. Bakajin, *Proc. Natl. Acad. Sci. U. S. A.*, 2008, **105**, 17250-17255.
2 X. J. Gong, J. Y. Li, H. J. Lu, R. Z. Wan, J. C. Li, J. Hu and H. P. Fang, *Nat. Nanotechnol.*, 2007, **2**, 709-712.
3 T. Jovanovic-Talisman, J. Tetenbaum-Novatt, A. S. McKenney, A. Zilman, R. Peters, M. P. Rout and B. T. Chait, *Nature*, 2009, **457**, 1023-1027.
4 P. Stroeve and N. Ileri, *Trends Biotechnol.*, 2011, **29**, 259-266.
5 X. Hou, W. Guo and L. Jiang, *Chem. Soc. Rev.*, 2011, **40**, 2385-2401.
6 Y. H. Zhou, W. Guo and L. Jiang, *Sci. China-Phys. Mech. Astron.*, 2014, **57**, 836-843.
7 L. J. Cheng and L. J. Guo, *Chem. Soc. Rev.*, 2010, **39**, 923-938.
8 J. C. T. Eijkel and A. van den Berg, *Chem. Soc. Rev.*, 2010, **39**, 957-973.
9 W. Sparreboom, A. van den Berg and J. C. T. Eijkel, *Nat. Nanotechnol.*, 2009, **4**, 713-720.
10 M. Tagliazucchi, Y. Rabin and I. Szleifer, *J. Am. Chem. Soc.*, 2011, **133**, 17753-17763.
11 I. Vlassiouk, S. Smirnov and Z. Siwy, *Nano Lett.*, 2008, **8**, 1978-1985.
12 D. Gillespie and S. Pennathur, *Anal. Chem.*, 2013, **85**, 2991-2998.
13 X. C. Xuan, *Electrophoresis*, 2008, **29**, 3737-3743.
14 Q. S. Pu, J. S. Yun, H. Temkin and S. R. Liu, *Nano Lett.*, 2004, **4**, 1099-1103.
15 S. J. Kim, Y. C. Wang, J. H. Lee, H. Jang and J. Han, *Phys. Rev. Lett.*, 2007, **99**. 044501
16 A. Plecis, R. B. Schoch and P. Renaud, *Nano Lett.*, 2005, **5**, 1147-1155.
17 R. Karnik, R. Fan, M. Yue, D. Y. Li, P. D. Yang and A. Majumdar, *Nano Lett.*, 2005, **5**, 943-948.
18 R. Karnik, K. Castelino and A. Majumdar, *Appl. Phys. Lett.*, 2006, **88**, 123114.
19 R. Fan, S. Huh, R. Yan, J. Arnold and P. D. Yang, *Nat. Mater.*, 2008, **7**, 303-307.
20 K. H. Paik, Y. Liu, V. Tabard-Cossa, M. J. Waugh, D. E. Huber, J. Provine, R. T. Howe, R. W. Dutton and R. W. Davis, *ACS Nano*, 2012, **6**, 6767-6775.
21 H. Zhang, X. Hou, L. Zeng, F. Yang, L. Li, D. Yan, Y. Tian and L. Jiang, *J. Am. Chem. Soc.*, 2013, **135**, 16102-16110.
22 X. Hou, F. Yang, L. Li, Y. Song, L. Jiang and D. Zhu, *J. Am. Chem. Soc.*, 2010, **132**, 11736-11742.
23 Y. Zhou, W. Guo, J. Cheng, Y. Liu, J. Li and L. Jiang, *Adv. Mater.*, 2012, **24**, 962-967.

24 W. J. Lan, D. A. Holden and H. S. White, *J. Am. Chem. Soc.*, 2011, **133**, 13300-13303.
25 M. Ali, B. Yameen, J. Cervera, P. Ramirez, R. Neumann, W. Ensinger, W. Knoll and O. Azzaroni, *J. Am. Chem. Soc.*, 2010, **132**, 8338-8348.
26 R. Karnik, C. H. Duan, K. Castelino, H. Daiguji and A. Majumdar, *Nano Lett.*, 2007, **7**, 547-551.
27 Y. He, D. Gillespie, D. Boda, I. Vlassiouk, R. S. Eisenberg and Z. S. Siwy, *J. Am. Chem. Soc.*, 2009, **131**, 5194-5202.
28 B. Yameen, M. Ali, R. Neumann, W. Ensinger, W. Knoll and O. Azzaroni, *J. Am. Chem. Soc.*, 2009, **131**, 2070-2071.
29 A. Siria, P. Poncharal, A. L. Biance, R. Fulcrand, X. Blase, S. T. Purcell and L. Bocquet, *Nature*, 2013, **494**, 455-458.
30 F. H. J. van der Heyden, D. J. Bonthuis, D. Stein, C. Meyer and C. Dekker, *Nano Lett.*, 2006, **6**, 2232-2237.
31 W. Guo, L. X. Cao, J. C. Xia, F. Q. Nie, W. Ma, J. M. Xue, Y. L. Song, D. B. Zhu, Y. G. Wang and L. Jiang, *Adv. Funct. Mater.*, 2010, **20**, 1339-1344.
32 J. K. Holt, H. G. Park, Y. M. Wang, M. Stadermann, A. B. Artyukhin, C. P. Grigoropoulos, A. Noy and O. Bakajin, *Science*, 2006, **312**, 1034-1037.
33 J. Chmiola, G. Yushin, Y. Gogotsi, C. Portet, P. Simon and P. L. Taberna, *Science*, 2006, **313**, 1760-1763.
34 K. P. Lee, H. Leese and D. Mattia, *Nanoscale*, 2012, **4**, 2621-2627.
35 C. H. Duan and A. Majumdar, *Nat. Nanotechnol.*, 2010, **5**, 848-852.
36 H. Chinen, K. Mawatari, Y. Pihosh, K. Morikawa, Y. Kazoe, T. Tsukahara and T. Kitamori, *Angew. Chem., Int. Ed.*, 2012, **51**, 3573-3577.
37 T. Tsukahara, A. Hibara, Y. Ikeda and T. Kitamori, *Angew. Chem. Int. Ed.*, 2007, **46**, 1180-1183.
38 W. Chen, Z. Q. Wu, X. H. Xia, J. J. Xu and H. Y. Chen, *Angew. Chem. Int. Ed.*, 2010, **49**, 7943-7947.
39 J. Cervera, V. Garcia-Morales and J. Pellicer, *J. Phys. Chem. B*, 2003, **107**, 8300-8309.
40 S. Z. Qian, B. Das and X. B. Luo, *J. Colloid Interface Sci.*, 2007, **315**, 721-730.
41 R. Qiao, J. G. Georgiadis and N. R. Aluru, *Nano Lett.*, 2006, **6**, 995-999.
42 M. Nagasawa, M. Tasaka and M. Tomita, *Neurosci. Lett.*, 1986, **66**, 19-24.
43 S. Hamann, J. J. Herrera-Perez, T. Zeuthen and F. J. Alvarez-Leefmans, *J. Physiol. (London)*, 2010, **588**, 4089-4101.
44 S.-J. Li, J. Li, K. Wang, C. Wang, J.-J. Xu, H.-Y. Chen, X.-H. Xia and Q. Huo, *ACS Nano*, 2010, **4**, 6417-6424.
45 C. J. Roy, C. Dupont-Gillain, S. Demoustier-Champagne, A. M. Jonas and J. Landoulsi, *Langmuir*, 2009, **26**, 3350-3355.
46 K. B. Jirage, J. C. Hulteen and C. R. Martin, *Anal. Chem.*, 1999, **71**, 4913-4918.
47 E. N. Savariar, K. Krishnamoorthy and S. Thayumanavan, *Nat. Nanotechnol.*, 2008, **3**, 112-117.
48 S. B. Lee and C. R. Martin, *Anal. Chem.*, 2001, **73**, 768-775.